

General Signal Model and Capacity Limit for Rydberg Quantum Information System

Jieao Zhu, *Student Member, IEEE* and Linglong Dai, *Fellow, IEEE*

Abstract—Rydberg atomic receivers represent a transformative approach to achieving high-sensitivity, broadband, and miniaturized radio frequency (RF) reception. However, existing static signal models for Rydberg atomic receivers rely on the steady-state assumption of atomic quantum states, which cannot fully describe the signal reception process of dynamic signals. To fill in this gap, in this paper, we present a general model to compute the dynamic signal response of Rydberg atomic receivers in closed form. Specifically, by applying small-signal perturbation techniques to the quantum master equation, we derive closed-form Laplace domain transfer functions that characterize the receiver's dynamic responses to time-varying signal fields. To gain more insights into the quantum-based RF-photocurrent conversion process, we further introduce the concept of quantum transconductance that describes the quantum system as an equivalent classical system. By applying quantum transconductance, we quantify the influence of in-band blackbody radiation (BBR) noise on the atomic receiver sensitivity. Extensive simulations for Rydberg atomic receivers validate the proposed signal model, and demonstrate the possibility of quantum receivers to outperform classical electronic receivers through the improvement of quantum transconductance.

Index Terms—Rydberg atomic receivers, dynamic response, quantum transconductance, blackbody radiation noise (BBR), sensitivity bounds.

I. INTRODUCTION

Classical electronic information systems have profoundly changed the world with their unprecedented capability of information acquisition and processing. Modern electronic systems, such as communication systems and radar systems, are capable of processing electromagnetic information, in which the physical process is mostly described by classical electrodynamics and thermodynamics. Unlike classical electronic systems, quantum information systems provide the possibility of breaking the fundamental limits of classical electronic systems by leveraging quantum phenomena [1, 2]. For example, by exploiting the quantum superposition phenomena, quantum computing is expected to achieve an exponential acceleration in comparison to classical computing [1]. By utilizing the quantum no-cloning theorem, quantum key distribution can achieve unconditioned secure quantum communication [3]. In addition, quantum sensing can achieve high sensitivity beyond

the capability of classical sensors, e.g., quantum electrometers [4].

On the road to quantum communication and sensing, Rydberg atomic receiver is a promising technology that has recently gained much research attention [4–8]. Unlike classical electronic receivers with metal antennas that convert radio-frequency (RF) signals to electronic signals, quantum receivers with Rydberg atoms convert RF signals to the change of atomic quantum states. Upon interacting with the external RF fields, the internal quantum states of these atoms are altered accordingly, resulting in a detectable change in the atom's optical transmission spectrum. This quantum phenomenon is known as the Autler-Townes (AT) effect [9] which can be observed in an electromagnetically induced transparency (EIT) experiment [10]. The optical change is then captured by subsequent photodetectors to generate electronic signals that carry information about the incident RF fields.

Due to the inherent high sensitivity of Rydberg states to RF fields, Rydberg atomic receivers can achieve weak signal detection that is expected to reach the quantum projection noise limit (QPNL) of $\sim 0.7 \text{ nV cm}^{-1} \text{ Hz}^{-1/2}$ [5], a level below the electronic thermal noise limit of around $3 \sim 5 \text{ nV cm}^{-1} \text{ Hz}^{-1/2}$ [11]. In addition, unlike electronic receivers that are designed for specific bands, quantum receivers can be tuned from several MHz [12] to GHz [13] and THz [14] with a single atomic vapor cell, which is impossible for state-of-the-art electronic receivers. Moreover, the small size of the atomic vapor cells (typically $\sim 2 \text{ cm}$) enables wavelength-independent RF receiving that overcomes Chu's limit [15] of classical antennas. These benefits of Rydberg atomic receivers [16] make them a promising quantum information system for different applications in wireless communications [8], sensing [17], astronomy [18], radar [19], etc.

A. Prior works

The Autler-Townes effect was originally discovered by S. H. Autler and C. H. Townes in [20], where the response of atomic spectra to external resonant fields was discussed. The first Rydberg atom-based electrometer was attributed to [21], where an E-field measuring apparatus based on Rydberg atoms was proposed. As a general purpose E-field sensor, the Rydberg atomic receiver has been quickly considered in different applications [16], from metrology [22] to wireless sensing [17, 19, 23] and wireless communications [13, 24–27]. Specifically, by leveraging the inherent sensitivity of Rydberg quantum sensors, the authors of [17] improved the wireless sensing accuracy by an order of magnitude. For wireless communications, researchers have realized AM signal reception [25], FM signal reception [26], QAM signal

This work was supported in part by the National Key Research and Development Program of China (Grant No. 2023YFB3811503), in part by the National Natural Science Foundation of China (Grant No. 62325106), and in part by the National Natural Science Foundation of China (Grant No. 62031019).

All authors are with the Department of Electronic Engineering, Tsinghua University, and the State Key Laboratory of Space Network and Communications, Tsinghua University, Beijing 100084, China (e-mails: zja21@mails.tsinghua.edu.cn, daill@tsinghua.edu.cn).

L. Dai is also with the EECS Department, Massachusetts Institute of Technology, Cambridge, MA 02139 USA.

reception [28], multi-band reception [27], continuous-band reception [13], and multi-carrier reception [24]. It should be pointed out that, most of these transmission techniques belong to the superheterodyne method [5, 12, 25, 27, 28], which is the most representative method that can achieve the state-of-the-art atomic reception sensitivity [29] with both amplitude and phase detection capability.

To understand the fundamental mechanisms and insights of atomic receivers, accurate signal models for each internal stage of the quantum system should first be established. The static signal model for atomic receivers was attributed to [5], where the concept of intrinsic gain κ (or intrinsic expansion coefficient [30]) was proposed to characterize the small-signal linear transfer coefficient from the signal Rabi frequency to the optical readout power. Based on this κ -coefficient, the wireless communication-oriented signal model for Rydberg atomic receivers was proposed in [6], where the atomic transfer relationship was derived by applying the static response [7, 31] to external RF fields. Following this approach, the authors of [8, 32] studied the large-signal case by treating the atomic receiver as a nonlinear RF envelope detector, and derived the linear range and channel capacities of the atomic receiver. Furthermore, to enable Rydberg atomic multiple-input multiple-output (MIMO) communications, the nonlinear point-to-point transmission model was extended to the MIMO transmission case [7, 31, 33].

However, the existing signal models for atomic receivers are static, i.e., they rely on the steady-state assumption [34] that the input signal remains unchanged until the quantum system reaches its steady state. For practical signal transmission, dynamic signal models for Rydberg atomic receivers are required. This general model for dynamic signal reception is absent from the existing literature. We point out that the difficulty in establishing such a dynamic signal model is caused by the *nonlinear response* determined by the quantum master equation, i.e., the atomic optical response is generally not a linear function of its RF input.

B. Our contributions

To fill in this gap, in this paper, we establish a general signal model that describes the dynamic Rydberg atomic response by applying the perturbation technique to linearize the master equation in the small-signal regime¹. The contributions of this paper are summarized as follows.

- Unlike traditional Rydberg analysis methods that rely on a static model, we propose a dynamic model for Rydberg atomic receivers by obtaining the perturbation solution to the quantum master equation. By analyzing this perturbation response with Laplace transform, a closed-form relationship between the optical response and the input RF signal is established, which is fully described by four Laplace domain transfer functions. To gain more insight into the general model, similar to the electronic transconductance of a transistor, we propose

the concept of *quantum transconductance* of a Rydberg atomic receiver.

- Based on the general model above, we analyze the atomic response to the inevitable in-band blackbody radiation (BBR) noise. Such analysis is not available for the existing static signal model. In addition to previous works that attribute noise to the imperfect optical readout and the standard quantum limit, we reveal that the BBR noise acts as another fundamental sensitivity performance limit to the atomic receivers, and that this sensitivity limit depends on a novel quantity called the BBR coherence factor. This coherence factor quantitatively describes the capability of BBR noise in corrupting the useful signal in the spatial domain.
- Simulations are conducted for both single-input single-output (SISO) and MIMO Rydberg atomic communication systems, taking into consideration the general signal model with BBR noise and other noise sources. Extensive numerical results are presented to justify the proposed dynamic signal models in both the continuous-time and discrete-time domains. Numerical results have also demonstrated the possibility of constructing a coherent quantum-MIMO receiver with improved capacity compared to classical electronic receivers.

C. Organization and Notation

Organization: The remainder of this paper is organized as follows. Section II introduces the basic quantum principles and system models of Rydberg atomic receivers. Section III computes the dynamic (transient) response of the atomic receivers to the time-varying external signal fields. Section IV discusses the influence of BBR on the atomic response. Section V presents the equivalent baseband model and simulation results. Finally, conclusions are drawn in Section VI.

Notation: bold uppercase characters \mathbf{X} denote matrices, with $[\mathbf{X}]_{mn}$ representing its (m, n) -th entry; bold lowercase characters \mathbf{x} denote vectors; \mathbf{I}_n denotes the identity matrix of size n ; \mathbf{X}^H , \mathbf{X}^T , and \mathbf{X}^* denotes Hermitian transpose, transpose, and complex conjugate of \mathbf{X} , respectively; for two operators \mathcal{A}_1 and \mathcal{A}_2 , $[\mathcal{A}_1, \mathcal{A}_2]$ denotes the commutator $\mathcal{A}_1\mathcal{A}_2 - \mathcal{A}_2\mathcal{A}_1$, and $\{\mathcal{A}_1, \mathcal{A}_2\}$ denotes their anti-commutator $\mathcal{A}_1\mathcal{A}_2 + \mathcal{A}_2\mathcal{A}_1$; \mathcal{F} denotes Fourier transform, and \mathcal{L} denotes the Laplace transform; For a time-domain signal $g(t)$, $g(i\omega)$ denotes its Fourier transform, and $g(s)$ denotes its Laplace transform; i is the imaginary unit; \hbar denotes the reduced Planck's constant; c_0 denotes the speed of light in a vacuum; ϵ_0 denotes the vacuum permittivity; η_0 denotes the vacuum wave impedance; $\text{vec}(\mathbf{X})$ stacks the columns of the matrix \mathbf{X} into a single column vector; $\text{PSD}[X(t)]$ denotes the double-sided power spectral density of the random process $X(t)$; For a real-valued bandpass signal $s(t)$, $s_a(t)$ denotes its analytic representation.

II. SYSTEM MODEL

In this section, we first describe the signal processing pipeline of the Rydberg atomic receiver. Then, we describe the atomic response to external radio frequency (RF) fields.

¹Simulation codes will be provided to reproduce the results in this paper: <http://oa.ee.tsinghua.edu.cn/dailinglong/publications/publications.html>.

Finally, we discuss the end-to-end electro-optical DC/AC responses of the atomic receiver.

A. Overall system description

Consider a Rydberg atomic receiver with the RF-sensitive capability provided by an atomic vapor cell filled with alkali atoms, e.g., cesium-133 atoms. The atoms in the vapor cell are exposed to four electromagnetic waves: the probe light $E_p(t)$ of angular frequency ω_p , the control light $E_c(t)$ of angular frequency ω_c , the RF local oscillator (LO) signal $E_{LO}(t)$ of angular frequency ω_{LO} , and the information-carrying RF signal $E_{sig}(t)$. All the EM fields are assumed to be co-polarized and represented by its complex envelope. To achieve state-of-the-art E-field sensitivity performance, we adopt the superheterodyne architecture proposed in [5] throughout this paper. In this receiver architecture, the frequency of the signal field $E_{sig}(t)$ is slightly different from that of $E_{LO}(t)$, where the frequency difference is defined as the intermediate frequency f_{IF} .

With a phase reference provided by the LO field, the time-varying signal field $E_{sig}(t)$ interacts with the alkali atoms, resulting in a change in the transmission coefficient of the probe light. The transmitted probe light is then fed into a photodetector, e.g., a photodiode, to generate the IF electronic signal for further processing. The signal flow chart is shown in Fig. 1, where it can be seen that the Rydberg atoms together with the photodetector act as a mixer [35] that down-converts the passband RF signal to the intermediate frequency f_{IF} with the help of $E_{LO}(t)$.

B. Quantum mechanisms for Rydberg atoms

The probe/control lights and the RF signal mainly drive the electron transition between four quantum states, which is denoted as $|1\rangle$, $|2\rangle$, $|3\rangle$, and $|4\rangle$. In this paper, the definitions of these energy levels are aligned to that of [5], which are $6S_{1/2}, F=4$; $6P_{3/2}, F=5$; $47D_{5/2}$ and $48P_{3/2}$. This four-energy level quantum system is described by an \hbar -normalized Hamiltonian, which is given by

$$\mathbf{H}(t) = \begin{bmatrix} 0 & \frac{\Omega_p}{2} & 0 & 0 \\ \frac{\Omega_p}{2} & -\Delta_p & \frac{\Omega_c}{2} & 0 \\ 0 & \frac{\Omega_c}{2} & -\Delta_p - \Delta_c & \frac{\Omega_{LO} + \Omega_{sig}^*(t)}{2} \\ 0 & 0 & \frac{\Omega_{LO} + \Omega_{sig}(t)}{2} & -\Delta_p - \Delta_c + \Delta_{LO} \end{bmatrix}, \quad (1)$$

where Ω_p , Ω_c , and Ω_{LO} are the Rabi frequencies of the probe field, control field, and the RF local oscillator (LO) field, respectively. Δ_p , Δ_c , and Δ_{LO} are the frequency detunings from resonance, where a positive detuning means the frequency is higher than resonance. Due to the presence of intermediate frequency f_{IF} , the signal Rabi frequency $\Omega_{sig}(t)$ is a complex-valued function of time [5], which is expressed as

$$\Omega_{sig}(t) = \frac{\mu_{RF} E_{sig}(t)}{\hbar} = \frac{\mu_{RF} E_{sig,0}}{\hbar} (I(t) + iQ(t)), \quad (2)$$

where $E_{sig,0}$ [V/m] is some reference level of the incident electric field, and μ_{RF} [Cm] is the transition dipole between

Rydberg states $|3\rangle$ and $|4\rangle$, and the real-valued oscillating RF field can be recovered from its analytic representation as

$$E_{sig,real}(t) = E_{sig,0} \cdot \text{Re}\{(I(t) + iQ(t))e^{i\omega_{LO}t}\}. \quad (3)$$

From a system-level viewpoint, the Rydberg atomic receiver operates as an electro-photon mixer, where the beat frequency of the two RF signals $E_{sig}(t)$ and $E_{LO}(t)$ is amplified and modulated to the intensity variation of the transmissive probe light. The transmissive probe light intensity is expressed as

$$P(t) = P_0 \exp\left(-2 \int_0^L \alpha(x, t) dx\right), \quad (4)$$

where P_0 [W] is the incident probe power, $P(t)$ is the time-dependent transmissive probe power, L [m] is the atomic electro-optical interaction length that equals the length of atomic vapor cell, and $\alpha(x, t)$ [m⁻¹] is the amplitude attenuation exponent per unit length at position $x \in [0, L]$ and time t . This attenuation exponent is related to the atomic quantum states via [5, 36]

$$\alpha(x, t) = -\frac{k_p N_0 \mu_{12}^2}{\epsilon_0 \hbar \Omega_p} \text{Im}\{\rho_{21}(x, t)\}, \quad (5)$$

where $k_p = \omega_p/c_0$ [m⁻¹] is the wavenumber of the probe light, N_0 [m⁻³] is the atomic density inside the vapor cell, μ_{12} is the transition dipole from $|1\rangle$ to $|2\rangle$, and $\rho_{21}(x, t)$ is the (2, 1)-th entry of the 4-by-4 Hermitian density matrix $\rho(x, t)$. The temporal evolution of the density matrix is fully described by the master equation

$$\frac{\partial \rho}{\partial t} = -i[\mathbf{H}, \rho] + D[\rho], \quad (6)$$

in which the decoherence operator $D[\rho]$ can be written as

$$D[\rho] = -\frac{1}{2}\{\mathbf{\Gamma}, \rho\} + \mathbf{\Lambda}[\rho], \quad (7)$$

where $\mathbf{\Gamma} = \text{diag}(0, \gamma_2, \gamma_3, \gamma_4)$, $\mathbf{\Lambda}[\rho] = \text{diag}(\gamma_2 \rho_{22} + \gamma_4 \rho_{44}, \gamma_3 \rho_{33}, 0, 0)$, and $\gamma_i, i = 2, 3, 4$ are the spontaneous decay rates of the i -th level [6].

As a first-order linear differential equation with variable coefficients, the master equation (6) determines the time evolution of $\rho_{21}(t)$. To better represent the time-domain signals, we decompose ρ_{21} into two terms $\bar{\rho}_{21} + \Delta\rho_{21}(t)$, where $\bar{\rho}_{21}$ denotes the time-averaged value of $\rho_{21}(t)$, and $\Delta\rho_{21}(t)$ is the time-varying part. The probe transmission power $P(t)$ and the attenuation exponent $\alpha(x, t)$ admit similar decompositions as

$$\begin{aligned} P(t) &= \bar{P} + \Delta P(t), \\ \alpha(x, t) &= \bar{\alpha}(x, t) + \Delta\alpha(x, t), \end{aligned} \quad (8)$$

where the time-averaged quantity x is denoted by \bar{x} in the rest part of this paper. After being detected by the photodiode, the output photocurrent $I_{ph}(t)$ of the photodiode is given by

$$I_{ph}(t) = \bar{I}_{ph} + \Delta I_{sig}(t) + \Delta I_n(t), \quad (9)$$

where \bar{I}_{ph} is the average value of the output photocurrent, $\Delta I_{sig}(t)$ is the photocurrent variation caused by the input E-field signal, and $\Delta I_n(t)$ denotes the total noise current. The

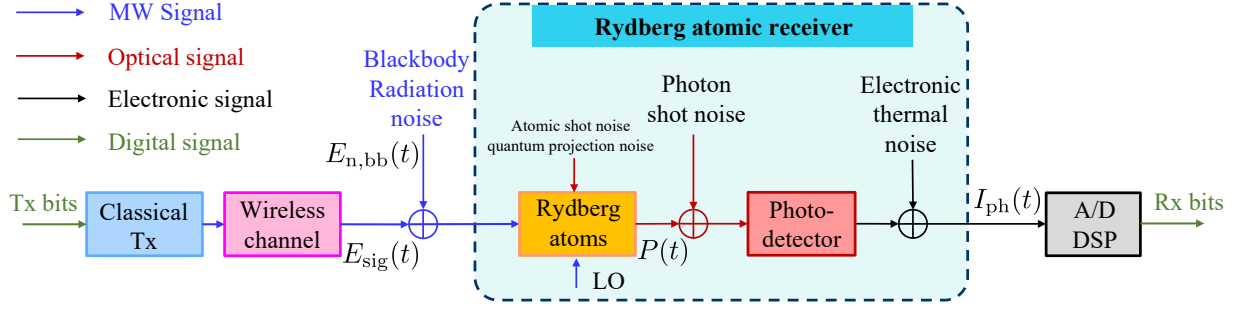


Fig. 1. Signal reception pipeline of Rydberg atomic receivers. The Rydberg atoms act as an electro-optical mixer that down-converts the passband RF signal to the IF. The Rydberg atomic receiver is composed of one atomic vapor cell and the subsequent analog-to-digital conversion (A/D) and digital signal processing (DSP) devices.

signal photocurrent is related to the optical signal power via

$$\Delta I_{\text{sig}}(t) = \frac{q_e \eta}{\hbar \omega_p} \Delta P(t), \quad (10)$$

where q_e is the elementary charge, η is the quantum efficiency of the photodiode, and ω_p is the angular frequency of the probe light.

C. Static DC and dynamic AC responses

From the communication engineering viewpoint, we are particularly interested in the input-output relation of the Rydberg atomic system. This relation is canonically separated into two parts: the DC transfer gain in the form of a differential input-output slope, and the dynamic AC transfer function in the form of a frequency response $H(i\omega)$. The DC transfer gain κ from the signal Rabi frequency $\Omega_{\text{sig}}(t)$ to the probe power variation $\Delta P(t)$ is first defined by the authors of [5], and has been studied theoretically in 2019 by the authors of [37] and examined experimentally in [30]. Analytical expressions of the DC gain can be found in many papers, e.g., in [5, 6, 23, 30, 37]. In fact, we can apply Mathematica to symbolically solve the steady-state master equation $d\rho/dt = 0$ for the steady-state solution $\bar{\rho}$ and extract its $(2, 1)$ -component to compute the DC probe transmission via (5). After obtaining the explicit expression of $\bar{\rho}_{21}$ as a function of E_{LO} , the DC gain κ can be computed by treating E_{sig} as small variations in E_{LO} , which leads to

$$\kappa = \frac{\partial \bar{P}}{\partial E_{\text{LO}}} \frac{\partial E_{\text{LO}}}{\partial \Omega_{\text{LO}}} = \frac{\hbar}{\mu_{\text{RF}}} \frac{\partial \bar{P}}{\partial E_{\text{LO}}}. \quad (11)$$

Thus, the DC gain is determined by the slope, i.e., the derivative, $\partial \bar{P} / \partial E_{\text{LO}}$ of the probe transmission-LO strength curve, as shown in Fig. 2.

Note that the dynamic AC response [38] can behave very differently from its DC counterpart, although the dynamic response is expected to be in agreement with the static response at $\omega = 0$. Since key communication performance indicators, like the system bandwidths and noise power spectral density (PSD), are fundamentally determined by the dynamic response of the system, we are devoted to evaluating the dynamic transfer function in the next section.

III. DYNAMIC MODELS

In this section, we find that the atomic receiver can be treated, up to a first-order approximation, as a linear time-

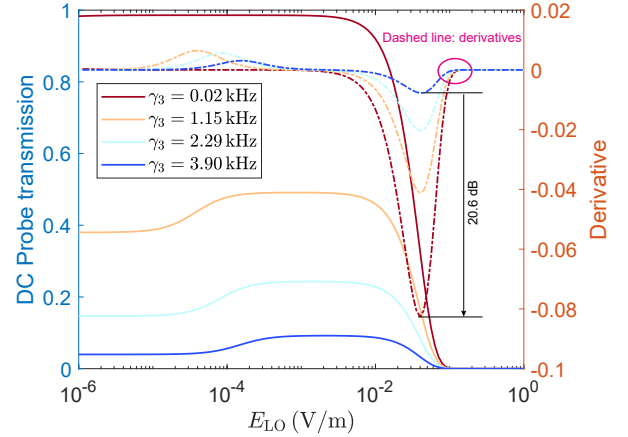


Fig. 2. DC probe transmission \bar{P}/P_0 as a function of the LO E-field E_{LO} [V/m]. Curves of the same color are respectively the \bar{P}/P_0 - E_{LO} curve (solid) and its derivative (dashed). The value of γ_4 is proportionally adjusted with γ_3 during simulation. These curves show a strong dependence of the DC gain κ on the inverse of Rydberg state lifetimes $\gamma_{3,4}$.

invariant (LTI) system. Specifically, we solve the transfer function of Rydberg atomic receivers by applying the small-signal perturbation technique to the master equation. The small-signal approximation holds when $E_{\text{sig}} \ll E_{\text{LO}}$.

A. Reformulation of the master equation

Since the master equation (6) is a first-order linear ordinary differential equation (ODE) in variable t , it can be reformulated into the standard matrix-vector form as

$$\frac{d\mathbf{x}_\epsilon}{dt} = (\mathbf{A}_0 + \epsilon \mathbf{A}_1(t)) \mathbf{x}_\epsilon(t), \quad (12)$$

where $\mathbf{x}_\epsilon(t) = \text{vec}(\rho) \in \mathbb{C}^{16}$ is the vectorized density matrix under small Hamiltonian perturbation $\epsilon \mathbf{A}_1(t)$, \mathbf{A}_0 is the unperturbed vectorized Hamiltonian given by

$$\mathbf{A}_0 = -i(\mathbf{I}_4 \otimes \mathbf{H}_0 - \mathbf{H}_0^\top \otimes \mathbf{I}_4) - \frac{1}{2}(\mathbf{\Gamma} \otimes \mathbf{I}_4 + \mathbf{I}_4 \otimes \mathbf{\Gamma}) + \gamma_2 \mathbf{E}_{1,6} + \gamma_4 \mathbf{E}_{1,16} + \gamma_3 \mathbf{E}_{6,11}, \quad (13)$$

\mathbf{H}_0 is the unperturbed Hamiltonian without the $\Omega_{\text{sig}}(t)$ term, and $\mathbf{E}_{ij} \in \mathbb{C}^{16 \times 16}$ denotes the matrix with the only “1” entry

located at (i, j) -th position. In the context of atomic receivers, the perturbation term is defined by $\Omega_{\text{sig}}(t)$ via

$$\epsilon \mathbf{A}_1(t) = -\frac{i}{2} [\mathbf{I}_4 \otimes (\Omega_{\text{sig}}(t) \mathbf{E}_{43} + \Omega_{\text{sig}}^*(t) \mathbf{E}_{34}) - (\Omega_{\text{sig}}(t) \mathbf{E}_{34} + \Omega_{\text{sig}}^*(t) \mathbf{E}_{43}) \otimes \mathbf{I}_4] \quad (14)$$

Generally, the reformulated master equation (12) can be solved by matrix exponents in the unperturbed case $\epsilon = 0$, where the unperturbed solution is

$$\mathbf{x}_0(t) = \exp(t \mathbf{A}_0) \mathbf{x}(0). \quad (15)$$

Note that the solution to (12) may be singular, i.e., a finite-energy perturbation $\epsilon \mathbf{A}_1(t)$ may lead to an infinite-energy differential response $\mathbf{x}_\epsilon(t) - \mathbf{x}_0(t)$. This phenomenon is caused by the zero eigenvalue of \mathbf{A}_0 , i.e., there exists some steady-state solution $\bar{\mathbf{x}} \in \mathbb{C}^{16}$ that satisfies $\mathbf{A}_0 \bar{\mathbf{x}} = \mathbf{0}$. Mathematically, this singularity can be eliminated by introducing an orthonormal basis transform \mathbf{Q} to the state vector \mathbf{x}_ϵ , which is expressed as

$$\mathbf{y}_\epsilon(t) := \mathbf{Q}^\top \mathbf{x}_\epsilon(t). \quad (16)$$

The orthonormal transform matrix \mathbf{Q} is designed to be

$$\mathbf{Q} = [\mathbf{u}_4, \mathbf{q}_1, \dots, \mathbf{q}_{15}], \quad (17)$$

where $\mathbf{u}_4 \in \mathbb{R}^{16}$ with four “1/2” entries located in the 1, 6, 11, 16-th positions, and $\mathbf{q}_k, k = 2, \dots, 15$ are arbitrarily chosen unit vectors that makes \mathbf{Q} an orthonormal matrix. The choice of \mathbf{u}_4 is related to the trace-preserving property of the master equation (6) that ensures $\mathbf{u}_4^\top \mathbf{A}_0 = \mathbf{0}$. The transformed master equation is expressed as

$$\begin{aligned} \frac{d\mathbf{y}_\epsilon(t)}{dt} &= \mathbf{Q}^\top (\mathbf{A}_0 + \epsilon \mathbf{A}_1(t)) \mathbf{Q} \mathbf{y}_\epsilon(t) \\ &:= (\mathbf{B}_0 + \epsilon \mathbf{B}_1(t)) \mathbf{y}_\epsilon(t). \end{aligned} \quad (18)$$

Due to the trace-preserving property of (6), the structure of the matrix \mathbf{B}_0 is

$$\mathbf{B}_0 = \begin{bmatrix} 0 & \mathbf{0}_{1 \times 15} \\ \mathbf{w}_0 & \mathbf{C}_0 \end{bmatrix}, \quad (19)$$

where $\mathbf{w}_0 \in \mathbb{C}^{15}$ and $\mathbf{C}_0 \in \mathbb{C}^{15 \times 15}$ are constant matrices determined by \mathbf{H}_0 and the choice of \mathbf{Q} . The same structure also applies to the perturbation term $\epsilon \mathbf{B}_1(t)$, yielding the definitions of $\epsilon \mathbf{w}_1(t)$ and $\epsilon \mathbf{C}_1(t)$. From the structure of $\mathbf{B}_0 + \epsilon \mathbf{B}_1(t)$, it can be seen that $d[\mathbf{y}_\epsilon]_1/dt = 0$, which yields $[\mathbf{y}_\epsilon]_1(t) \equiv [\mathbf{y}_\epsilon]_1(0) = \mathbf{u}_4^\top \mathbf{x}(0) = 1/2$. To study the time-varying properties of the remaining components of \mathbf{y}_ϵ , we let $\mathbf{z}_\epsilon = [\mathbf{y}_\epsilon]_{2:16} \in \mathbb{C}^{15}$. This yields, for any $\epsilon > 0$,

$$\frac{d\mathbf{z}_\epsilon}{dt} = \frac{1}{2} \mathbf{w}_0 + (\mathbf{C}_0 + \epsilon \mathbf{C}_1(t)) \mathbf{z}_\epsilon(t), \quad (20)$$

where the small-signal term $\epsilon \mathbf{w}_1(t)$ can be eliminated by properly choosing \mathbf{q}_k . One can check that all of the eigenvalues of \mathbf{C}_0 have negative real parts, indicating that (20) is non-singular against small perturbations $\epsilon \mathbf{C}_1(t)$.

B. Small-signal transfer function

After reformulation of the master equation into the stable form (20), the perturbation method can be applied to

evaluate the small-signal transfer function from the entries of $\epsilon \mathbf{C}_1(t)$ to the variations that appear in $\rho_{21}(t) = [\text{unvec}(\mathbf{Q}[1/2, \mathbf{z}(t)^\top]^\top)]_{21}$. Starting from (20), we assume the ϵ -perturbed solution to be

$$\mathbf{z}_\epsilon(t) = \mathbf{z}_0(t) + \epsilon \left. \frac{\partial \mathbf{z}_\epsilon}{\partial \epsilon} \right|_{\epsilon=0} + o(\epsilon). \quad (21)$$

Substitute this first-order approximated solution into (20), we get

$$\begin{aligned} \frac{d\mathbf{z}_0}{dt} + \epsilon \frac{\partial}{\partial t} \frac{\partial \mathbf{z}_\epsilon}{\partial \epsilon} &= \frac{1}{2} \mathbf{w}_0 + \mathbf{C}_0 \mathbf{z}_0(t) \\ &+ \epsilon \left(\mathbf{C}_1(t) \mathbf{z}_0(t) + \mathbf{C}_0 \frac{\partial \mathbf{z}_\epsilon}{\partial \epsilon} \right) + o(\epsilon), \end{aligned} \quad (22)$$

where $o(\epsilon)$ denotes terms that vanish after dividing by ϵ as $\epsilon \rightarrow 0$. We know that $\mathbf{z}_0(t)$ satisfies the unperturbed differential equation $d\mathbf{z}_0/dt = \mathbf{C}_0 \mathbf{z}_0 + \mathbf{w}_0/2$, thus we get

$$\frac{\partial}{\partial t} \left(\frac{\partial \mathbf{z}_\epsilon}{\partial \epsilon} \right) = \mathbf{C}_1(t) \mathbf{z}_0(t) + \mathbf{C}_0 \left(\frac{\partial \mathbf{z}_\epsilon}{\partial \epsilon} \right). \quad (23)$$

This is a first-order constant-coefficient matrix-vector differential equation of unknown vector $\partial \mathbf{z}_\epsilon / \partial \epsilon$, where the solution can be expressed as

$$\left. \frac{\partial \mathbf{z}_\epsilon}{\partial \epsilon} \right|_{\epsilon=0}(t) = \int_0^t \exp((t-\tau) \mathbf{C}_0) \mathbf{C}_1(\tau) \mathbf{z}_0(\tau) d\tau. \quad (24)$$

The equation (24) describes the first-order dynamic response of the Rydberg atomic receiver, expressed in terms of a convolution of the matrix exponential $\exp(t \mathbf{C}_0)$ with the product of the input excitation term $\mathbf{C}_1(t)$ and the unperturbed solution $\mathbf{z}_0(t)$. Multiply both sides of (24) with ϵ and take the Laplace transform, the s -domain small-signal response of the atomic receiver is given by

$$\begin{aligned} \mathcal{L}[\epsilon \frac{\partial \mathbf{z}_\epsilon}{\partial \epsilon}](s) &\stackrel{(a)}{=} \mathcal{L}[e^{t \mathbf{C}_0}](s) \cdot (\epsilon \mathbf{C}_1(s)) \cdot \bar{\mathbf{z}}_0 \\ &= (s \mathbf{I}_{15} - \mathbf{C}_0)^{-1} (\epsilon \mathbf{C}_1(s)) \bar{\mathbf{z}}_0, \end{aligned} \quad (25)$$

where (a) comes from the assumption that the Rydberg atomic system have reached steady-state before E_{sig} is applied. The term $\epsilon \mathbf{C}_1(s)$ is the Laplace transform of the time-domain perturbation $\epsilon \mathbf{C}_1(t)$, and $\bar{\mathbf{z}}_0$ is the steady-state solution to (20) with $\epsilon = 0$, which is given by.

$$\bar{\mathbf{z}}_0 = -\frac{1}{2} \mathbf{C}_0^{-1} \mathbf{w}_0. \quad (26)$$

By undoing the applied linear transforms in $\mathbf{z}_\epsilon(t)$, the transfer function of any variation in the Hamiltonian $\epsilon \mathbf{H}_1(t)$ to the variations in any element of the density matrix $[\Delta \rho_{mn}]_{4 \times 4}$ can be easily computed. In the case of Rydberg atomic receivers, we are particularly interested in $\Delta \rho_{21}$, since it fully describes the probe transmission coefficient.

Let $\mathbf{T}(s) := [T_{k\ell}(s)]_{4 \times 4}$ denote the transfer functions from $\epsilon \mathbf{H}_1(t)$ to $\Delta \rho_{21}$. Then, $\mathbf{T}(s)$ is expressed as

$$T_{k\ell}(s) = \left[\mathbf{Q} \begin{bmatrix} \mathbf{0} \\ \mathbf{I}_{15} \end{bmatrix} (s \mathbf{I}_{15} - \mathbf{C}_0)^{-1} \frac{\partial (\epsilon \mathbf{C}_1)}{\partial [\epsilon \mathbf{H}_1]_{k\ell}} \bar{\mathbf{z}}_0 \right]_2. \quad (27)$$

Since the input signal only alters $[\mathbf{H}_1]_{34}$ and $[\mathbf{H}_1]_{43}$, the two entries T_{34} and T_{43} contribute to the end-to-end electro-

optical response of the atomic receiver. Rewrite the signal Rabi frequency (2) in terms of the analytic baseband signal $X(t) := I(t) + iQ(t)$, then the Laplace transform of the atomic response $\Delta\rho_{21}(t)$ is expressed as

$$\mathcal{L}[\Delta\rho_{21}](s) = \frac{\mu_{\text{RF}} E_{\text{sig},0}}{2\hbar} \times [T_{34}(s)(I(s) - iQ(s)) + T_{43}(s)(I(s) + iQ(s))], \quad (28)$$

where $I(s)$ and $Q(s)$ are Laplace transforms of $I(t)$ and $Q(t)$, respectively. We can separate the total gain into two parts: The in-phase gain $G_I(s)$ and the quadrature gain $G_Q(s)$, which are given by

$$\begin{aligned} G_I(s) &= \frac{\mu_{\text{RF}}}{2\hbar} (T_{43}(s) + T_{34}(s)) \\ G_Q(s) &= \frac{i\mu_{\text{RF}}}{2\hbar} (T_{43}(s) - T_{34}(s)). \end{aligned} \quad (29)$$

To separate the real-part response of $\Delta\rho_{21}$ from the imaginary-part response, we separate the real-part filter and imaginary-part filter of both $G_I(s)$ and $G_Q(s)$ as

$$\begin{aligned} G_I(s) &= G_{I,1}(s) + iG_{I,2}(s), \\ G_Q(s) &= G_{Q,1}(s) + iG_{Q,2}(s). \end{aligned} \quad (30)$$

This separation is done by extracting the real- and imaginary-part of the numerator polynomial coefficients of $G_I(s)$ and $G_Q(s)$. Note that the system characteristic polynomial (denominator polynomial) $p(s) := \det(s\mathbf{I}_{15} - \mathbf{C}_0)$ is always a real-coefficient polynomial, i.e., the complex system poles always appear in conjugate pairs. With these four separated gains, the real- (imaginary-) part response of $\Delta\rho_{21}$ is given by

$$\mathcal{L} \begin{bmatrix} \text{Re}\{\Delta\rho_{21}\} \\ \text{Im}\{\Delta\rho_{21}\} \end{bmatrix} = E_{\text{sig},0} \begin{bmatrix} G_{I,1}(s) & G_{Q,1}(s) \\ G_{I,2}(s) & G_{Q,2}(s) \end{bmatrix} \cdot \begin{bmatrix} I(s) \\ Q(s) \end{bmatrix} \quad (31)$$

In the near-resonance regime where the laser detunings, the RF LO detuning and the intermediate frequency f_{IF} are all small, we numerically observe that G_Q is significantly smaller than G_I , and G_I is nearly purely imaginary. This means the $G_{I,2}$ component is significantly larger than other three components, i.e., the Rydberg atoms respond only to the in-phase component of E_{sig} and ignore the quadrature component. This observation is somehow in accordance with the non-coherent amplitude receiving model that appear in [6, 7].

C. Quantum transconductance

In the previous subsection, we have theoretically computed the transfer function from $X(t)$ to $\Delta\rho_{21}(t)$. In this subsection, we introduce a novel concept of “quantum transconductance” to fully describe the transient response from the input E-field $E_{\text{sig}}(t)$ to the output signal photocurrent $\Delta I_{\text{sig}}(t)$ after photo-electric conversion of the photodiode. This quantum transconductance is analogous to the transconductance of an RF transistor that is key to an RF low-noise amplifier (LNA).

We define the time-domain quantum transconductance $g_q(x, \tau)$ to be the impulse response from the in-phase component of the signal E-field $\text{Re}\{E_{\text{sig}}(t)\}$ [V/m] to the output photocurrent change $\Delta I_{\text{sig}}(t)$ [A] per unit electro-atomic interaction length dx [m]. Note that this time-domain quantum

transconductance have a dimension of [S · Hz]. By definition of the quantum transconductance, we have

$$\Delta I_{\text{sig}}(t) = \int_0^L dx \int_0^t d\tau g_q(x, \tau) \text{Re}\{E_{\text{sig}}\}(x, t - \tau), \quad (32)$$

where the s -domain quantum transconductance can be obtained by taking the Laplace transform of both sides, which yields

$$\Delta I_{\text{sig}}(s) = \int_0^L g_q(x, s) E_{\text{sig},0} I(x, s) dx. \quad (33)$$

This s -domain quantum transconductance $g_q(x, s)$ does have a dimension of conductance [S]. To compute $g_q(x, s)$, we note that the variations in the probe transmission (4) is determined by the variation in the attenuation constant $\Delta\alpha(x, t)$, which is further determined by the variations in the imaginary part of $\Delta\rho_{21}(x, t)$. Thus, by applying all the relationships (4), (5), and (29), the quantum transconductance is expressed in the frequency domain $s = i\omega$ as

$$\begin{aligned} g_q(x, i\omega) &:= \frac{d^2(\Delta I_{\text{sig}})}{dE_{\text{sig}} dx} \\ &= \frac{q_e \eta}{\hbar \omega_p} \cdot \bar{P} \cdot \frac{2k_p N_0 \mu_{12}^2}{\epsilon_0 \hbar \Omega_p(x)} \cdot G_{I,2}(x, i\omega) \\ &\approx \bar{I}_{\text{ph}} \cdot \frac{2k_p N_0 \mu_{12}^2}{\epsilon_0 \hbar \Omega_p(x)} \cdot G_{I,2}(x, i\omega), \end{aligned} \quad (34)$$

where \bar{I}_{ph} is the DC photocurrent when the signal field is not applied. One can also relate $\Delta I_{\text{sig}}(i\omega)$ to the Fourier transform of the input signal $E_{\text{sig}}(x, i\omega)$ via

$$\Delta I_{\text{sig}}(i\omega) = \int_0^L g_q(x, i\omega) \frac{E_{\text{sig}}(x, i\omega) + E_{\text{sig}}^*(x, -i\omega)}{2} dx. \quad (35)$$

From this equation, we can see that the mirror frequency at $-i\omega$ also contributes to the probe response. We note that, in the case where $E_{\text{sig}}(x, i\omega)$ is completely within the upper sideband, the expression of the photocurrent response $\Delta I_{\text{sig}}(t)$ can be simplified to be $\Delta I_{\text{sig},a}(t) = \int_0^L (g_q(x, \tau) * E_{\text{sig}}(x, \tau))|_{\tau=t} dx$, where $*$ denotes convolution.

Generally, g_q depends on x through the probe Rabi frequency $\Omega_p(x)$. This dependence is caused by the reduction of $\Omega_p(x)$ as a function of x caused by probe attenuation. For small vapor cells with short interaction length L , this dependence is somehow weakened.

Remark 1. The transient probe response is mainly described by $G_{I,2}$ in (31), whose constant multiple is defined as the quantum transconductance (34). The quantum transconductance for other components can be similarly defined by applying the factor $2k_p N_0 \mu_{12}^2 \bar{I}_{\text{ph}} / (\epsilon_0 \hbar \Omega_p)$ to the other three transfer functions in (31), but they are significantly smaller than $G_{I,2}$, as will be verified in the numerical results section.

D. Alternative definition of the Rydberg intrinsic gain

The authors of [5, 8] define the response of the Rydberg atomic receiver to a single-tone input to be

$$P(t) = \bar{P} + \kappa |\Omega_{\text{sig}}| \cos(2\pi f_{\text{IF}} t + \theta), \quad (36)$$

where κ is the intrinsic gain of the Rydberg system with unit $[\text{W Hz}^{-1}]$, and θ is the phase of the signal field. Here we extend this intrinsic gain κ into the frequency-dependent version $\kappa(i\omega)$. Assuming a uniform signal field across the quantum aperture $[0, L]$, the new definition of κ is naturally related to $G_{I,2}(x, i\omega)$ by

$$\kappa(i\omega) = \bar{P} \int_0^L \frac{2k_p N_0 \mu_{12}^2}{\epsilon_0 \hbar \Omega_p(x)} G_{I,2}(x, i\omega) dx, \quad (37)$$

where $\omega = 2\pi f_{\text{IF}}$. Note that for $\omega = 0$, the definition and computation formulas of the DC intrinsic gain $\kappa(i0)$ are in alignment with the theoretical work in [8]. A straightforward numerical computation of the DC gain $\kappa(i0)$ yields the result of $-8.67 \times 10^{-13} [\text{W/Hz}]$, which is aligned with the measurement result in [30, Table. 1].

Furthermore, the frequency-dependent intrinsic gain is related to the quantum transconductance $g_q(x, i\omega)$ via

$$\kappa(i\omega) = \frac{\hbar \omega_p}{q_e \eta} \int_0^L g_q(x, i\omega) dx. \quad (38)$$

Compared to the frequency-dependent intrinsic gain $\kappa(i\omega)$, the proposed quantum transconductance $g_q(x, i\omega)$ is x -dependent. Since the blackbody radiation (BBR) exhibits strong spatial correlation with coherence length $\sim \lambda/2$ [39, 40], this coordinate-dependent property of $g_q(x, i\omega)$ enables the subsequent blackbody radiation noise analysis of the atomic receiver.

IV. NOISE MODELS

Noises that affect Rydberg atomic receivers can be generally divided into two categories: the external noises, and the internal noises. While internal noises can be actively suppressed by optimized designs of the receiver, external noises pose intrinsic limits to the atomic receiver, since the receivers cannot distinguish in-band external noises from the desired signals. In this section, we study how the external in-band blackbody radiation noises affect the response of the atomic receiver.

A. Properties of the blackbody radiation

Blackbody radiation is the wide-spectrum radiation emitted by any object above absolute zero temperature. In the normal temperature environment of $T = 300 \text{ K}$, blackbody radiation contributes to most part of the electronic noise observed by classical RF receivers, since it directly interacts with the RF antenna and creates an equivalent noise source in the first stage of classical RF signal processing pipeline before the low-noise amplifier (LNA). In an isotropic blackbody radiation field of temperature T , the spectral radiance is given by

$$B_\nu(T) = \frac{2\nu^2}{c^2} \cdot \frac{h\nu}{\exp(h\nu/(k_B T)) - 1} \quad [\text{W Hz}^{-1} \text{ m}^{-2} \text{ rad}^{-1}], \quad (39)$$

where ν is the center frequency that the blackbody radiation measurement is performed. At room temperature, this spectral radiance is well-approximated by $2\nu^2 k_B T / c^2$. To compute the atomic response to the blackbody radiation, we need to first

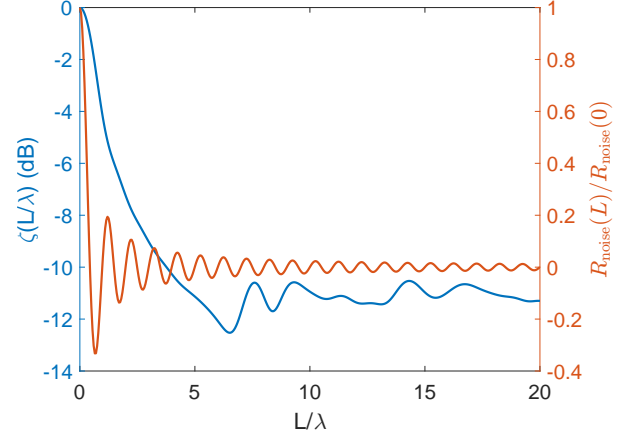


Fig. 3. Coherence factor $\zeta(\ell)$ and normalized noise correlation $R_n(\ell, i0)$ as a function of normalized interaction length ℓ . The fluctuation of $\zeta(\ell)$ in the large- ℓ regime is caused by the long-tail effect in the noise correlation.

compute the per-Hertz electric field phasor as the E-field input $E_{\text{sig}}(x, i\omega)$ in (32). By noticing the plane-wave power flux formula $S = |E_{\text{sig}}|^2 / (2\eta_0)$, we write the unit-solid angle unit-frequency blackbody radiation field at point \mathbf{x} along incidence direction $\hat{\mathbf{r}}$ to be

$$d\mathbf{E}_\nu(\mathbf{x}, \hat{\mathbf{r}}) = \sqrt{\eta_0 B_\nu(T, \hat{\mathbf{r}})} e^{ik_0 \hat{\mathbf{r}} \cdot \mathbf{x}} (W_1(\hat{\mathbf{r}}) \hat{\mathbf{t}}_1 + W_2(\hat{\mathbf{r}}) \hat{\mathbf{t}}_2) dS(\hat{\mathbf{r}}), \quad (40)$$

where $\hat{\mathbf{r}}, \hat{\mathbf{t}}_1, \hat{\mathbf{t}}_2$ constitutes an orthonormal basis of \mathbb{R}^3 , W_1, W_2 are two independent complex white Gaussian random fields of unit variance on the unit sphere S^2 , and $dS(\hat{\mathbf{r}})$ is the standard spherical measure that integrates to 4π . The total strength of the all-directional noise field is given by $\mathbf{E}_\nu(\mathbf{x}) = \int_{4\pi} d\mathbf{E}_\nu(\mathbf{x}, \hat{\mathbf{r}})$. Note that this total field further induces a spatial correlation function given by

$$\mathbf{R}_{\mathbf{E}_\nu}(\mathbf{x}, \mathbf{x}') := \mathbb{E} [\mathbf{E}_\nu(\mathbf{x}) \mathbf{E}_\nu^H(\mathbf{x}')] \quad [\text{V}^2 \text{ m}^{-2} \text{ Hz}^{-1}], \quad (41)$$

where $\mathbb{E}[\cdot]$ denotes ensemble average. This quantity can be analytically computed to be

$$\mathbf{R}_{\mathbf{E}_\nu}(\mathbf{x}, \mathbf{x}') = \pi \eta_0 B_\nu(T) \times [(f_0(\beta) + f_2(\beta)) \mathbf{I}_3 + (f_0(\beta) - 3f_2(\beta)) \hat{\mathbf{r}} \hat{\mathbf{r}}^T], \quad (42)$$

where $f_n(\beta) := \int_{-1}^1 x^n e^{i\beta x} dx$, $\beta = k_L O r$, $r = \|\mathbf{x} - \mathbf{x}'\|$, and $\hat{\mathbf{r}} = (\mathbf{x} - \mathbf{x}')/r$, and \cdot . The same spatial correlation formula of blackbody radiation fields can be found in [39, 41, 42]. Intuitively, if the blackbody radiation field correlation is stronger, then it will add up coherently from $x = 0$ to $x = L$, resulting in a stronger influence on the output of Rydberg atomic receivers. This intuition will be justified by quantitative computations in the next subsection.

B. Atomic response to the blackbody radiation

Let $E_n(x, i\omega)$ be the blackbody radiation noise field phasor with unit $\text{V m}^{-1} \text{ Hz}^{-1/2}$. The atomic response to this noise, in terms of the power spectral density (PSD) $P_{\Delta I_{n, \text{bb}}}(\omega) [\text{A}^2 \text{ Hz}^{-1}]$ of the noise-induced photocurrent, is

defined at IF angular frequency $\omega \neq 0$ as

$$\begin{aligned} P_{\Delta I_{n,bb}}(\omega) &:= \text{PSD}[\Delta I_{bb}(t)](\omega) \\ &= \iint_{[0,L]^2} dx_1 dx_2 g_q(x_1, i\omega) g_q^*(x_2, i\omega) \times \\ &\mathbb{E} \left[\frac{(E_n(x_1, i\omega) + E_n^*(x_1, -i\omega))(E_n^*(x_2, i\omega) + E_n(x_2, -i\omega))}{4} \right]. \end{aligned} \quad (43)$$

By applying the noise correlation formula $\mathbb{E}[E_n(x_1, i\omega_1) E_n^*(x_2, i\omega_2)] = R_n(x_1 - x_2, i\omega_1) \mathbf{1}_{\omega_1 = \omega_2}$, we compute the noise current PSD to be

$$\begin{aligned} P_{\Delta I_{n,bb}}(\omega) &\stackrel{(a)}{\approx} \frac{|g_q(i\omega)|^2}{4} \times \\ &\iint_{[0,L]^2} (R_n(x_1 - x_2, i\omega) + R_n(x_2 - x_1, -i\omega)) dx_1 dx_2 \\ &\stackrel{(b)}{\approx} \frac{|Lg_q(i\omega)|^2}{2} \cdot \frac{1}{L^2} \int_{-L}^L (L - |u|) R_n(u, 0) du, \end{aligned} \quad (44)$$

where the approximation (a) holds for small electro-optical interaction length L , the approximation (b) is justified by approximating $R_n(u, \pm i\omega)$ with $R_n(u, 0)$ for small intermediate frequency $|\omega| \ll 2\pi f_{LO}$, and $R_n(u, i\omega)$ is the z -direction noise correlation function at spatial separation u , which can be computed by taking the (3, 3)-th entry in (41). Since the noise variance is intimately related to the asymptotic rate of BBR coherence decay as a function of ℓ , we define the coherence factor $\zeta(\ell)$ to be

$$\begin{aligned} \zeta(\ell) &= \frac{1}{L^2 R_n(0, i0)} \int_{-L}^L (L - |u|) R_n(u, i0) du \\ &= \frac{1}{\ell^2 R_n(0, i0)} \int_{-\ell}^{\ell} (\ell - |u'|) R_n(\lambda_{LO} u', i0) du', \end{aligned} \quad (45)$$

where $\ell := L/\lambda_{LO}$ is the electro-optical interaction length normalized by LO wavelength. One can check that this coherence factor only depends on $\ell = L/\lambda_{LO}$ instead of L , and that it satisfies $0 < \zeta(\ell) < 1$. When $\ell \rightarrow 0$, the spatial correlation becomes almost fully coherent, and thus $\zeta(\ell)$ will be close to 1. The coherence factor and the normalized noise correlation function are shown in Fig. 3.

With the concept of the spatial coherence factor $\zeta(\ell)$, the PSD of the atomic response current (variance of the output photoelectric current per unit bandwidth) to the noise field is further simplified to be

$$P_{\Delta I_{n,bb}}(\omega) = \frac{4\pi}{3} \eta_0 B_\nu(T) \zeta \left(\frac{L}{\lambda_{LO}} \right) L^2 |g_q(i\omega)|^2, \quad (46)$$

where $R_n(0, i\omega)$ is expressed in terms of the spectral radiance $B_\nu(T)$ via (42). Note that the PSD value (46) is only a lower bound in practical Rydberg atomic receivers. In real-world quantum receivers, the internal noises including photon shot noise, atomic collision noise, atomic transition noise, and Johnson-Nyquist noise should also be considered, resulting in a larger noise variance (see Fig. 1 for the noise introduction points in the system). Note that the out-of-band BBR noises that are resonant to other Rydberg-Rydberg transitions have already been considered in the form of dephasing coefficients

$\gamma_{3,4}$ [6, 43].

Assume that the received signal $E_{sig}(i\omega)$ completely lies in the upper sideband (USB) with $\omega > 0$, such that there is no mirror frequency interference at $\omega < 0$. Combining the above BBR noise variance with the signal transfer relationship (33), we compute the best achievable receive signal-to-noise ratio (SNR) at IF angular frequency $\omega > 0$ to be

$$\text{SNR}_q^*(\omega) = \frac{\frac{1}{4} P_{sig}(\omega)}{\frac{4\pi}{3} \eta_0 B_\nu(T) \zeta(L/\lambda_{LO})}, \quad (47)$$

where $P_{sig}(\omega)$ [$V^2 \text{ m}^{-2} \text{ Hz}^{-1}$] is the double-sided power spectral density of the infinitely long *analytic* input signal $E_{sig}(t)$, and the blackbody spectral radiance B_ν is evaluated at $\nu = f_{LO}$. The factor 1/4 is explained by the selective response to the in-phase component $I(t)$ of the Rydberg atomic receivers and the definition of double-sided PSD.

C. Sensitivity analysis

Another popular performance measure of the Rydberg atomic receiver is the minimum detectable E-field. By setting the SNR in (47) to 0 dB, we get the lower bound of the per-second detectable in-phase E-field strength to be

$$E_{I,min} \geq \sqrt{\frac{4\pi}{3} \eta_0 B_\nu(T) \zeta(\ell)} \quad [\text{V m}^{-1} \text{ Hz}^{-1/2}]. \quad (48)$$

A straightforward computation at $T = 300\text{K}$, $f_{LO} = 6.9458\text{ GHz}$ with $\zeta = 1$ yields the value of $E_{I,min} \geq 838\text{ pV cm}^{-1} \text{ Hz}^{-1/2}$, while this value can be improved by increasing the length of electro-atomic interaction L . This blackbody radiation-determined value is comparable to the quantum projection noise limit (QPNL)-determined sensitivity of $\sim 700\text{ pV cm}^{-1} \text{ Hz}^{-1/2}$ [5]. Although a measured sensitivity of $\sim 55\text{ nV cm}^{-1} \text{ Hz}^{-1/2}$ [5] and $10.0\text{ nV cm}^{-1} \text{ Hz}^{-1/2}$ [29] are reported, which is about 20 dB worse than state-of-the-art classical electronic receivers [6], we anticipate that the sensitivity of Rydberg atomic receivers will finally approach the lower bound that is jointly determined by (48) and the QPNL sensitivity bound.

D. Noise PSD in the output power of the photodiode

In most of the applications, it is more beneficial to know the electronic noise parameters in terms of the PSD of the noise current, since this PSD can be directly measured by the spectrum analyzers. The opto-electronic signal processing pipeline of Rydberg atomic receiver is shown in Fig. 4.

The small-signal output photocurrent $\Delta I_{ph}(t)$ is expressed in the time domain as

$$\Delta I_{ph}(t) = \Delta I_{sig}(t) + \Delta I_{n,bb}(t) + \Delta I_{n,R_s}(t) + \Delta I_{n,shot}(t), \quad (49)$$

where $\Delta I_{sig}(t)$ is determined by the input signal E-field through (32), the PSD of $\Delta I_{n,bb}(t)$ is lower-bounded by (46), the PSD of $\Delta I_{n,R_s}(t)$ equals $2k_B T/R_s$ with R_s being the DC-biasing resistance in series with the photodiode, and $\Delta I_{n,shot}(t)$ is the photon shot noise with PSD given by

$$\text{PSD}[\Delta I_{n,shot}(t)](\omega) = q_e \bar{I}_{ph}. \quad (50)$$

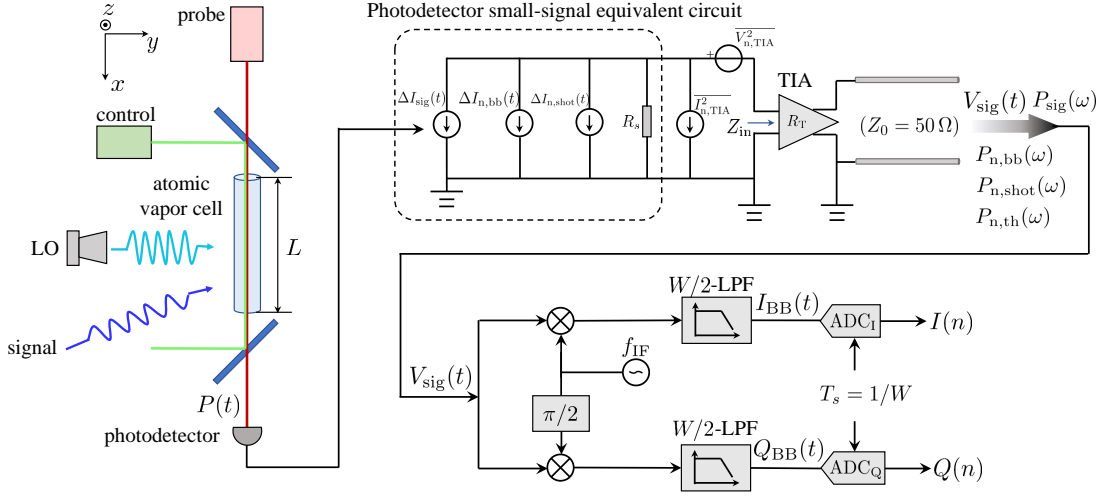


Fig. 4. Analog signal processing pipeline for Rydberg atomic receivers: Photo-atomic interaction, transimpedance amplification (TIA), and IQ down-conversion.

Note that the photon shot noise is caused by the discreteness of the Poisson photon arrival process. To convert this current PSD into the output PSD of the transimpedance amplifier (TIA), we assume that the TIA (FEMTO DHPCA-100 [44]) has a transimpedance of $R_T = 10 \text{ k}\Omega$, an input referred current noise level of $I_{n,\text{TIA}} = 1.8 \text{ pA Hz}^{-1/2}$, an input referred voltage noise level of $V_{n,\text{TIA}} = 2.8 \text{ nV Hz}^{-1/2}$, and an input impedance of $Z_{\text{in}} = 60 \Omega$. The photodetector is assumed to be a reverse-biased photodiode in series of a resistor $R_s = 1 \text{ k}\Omega$ that is connected to the supply voltage. The TIA output is connected to a matched load of $R_L = 50 \Omega$ [30], e.g. a spectrum analyzer.

With these assumptions, the conversion formula from the photocurrent noise PSD to the TIA output noise PSD given by

$$P_{n,\text{out}}(\omega) = \text{PSD}[\Delta I](\omega) \times \frac{(R_T K_c)^2}{R_L} \quad (51)$$

where $P_{n,\text{out}}(\omega)$ is the double-sided output noise power spectral density of the TIA measured in W/Hz , $K_c = R_s/(R_s + Z_{\text{in}})$ is the current divider coefficient at the TIA input, and $\text{PSD}[\Delta I](\omega)$ is in A^2/Hz . Note that $\text{PSD}[\Delta I](\omega)$ can represent both the BBR-induced noise and the photon shot noise. Thus, $P_{n,\text{out}}$ can represent both $P_{n,\text{bb}}$ and $P_{n,\text{shot}}$. Moreover, the circuit total thermal noise (Johnson-Nyquist noise and the amplifier noise) PSD can be computed by

$$P_{n,\text{th}}(\omega) = \frac{R_T^2}{2R_L} \left(I_{n,\text{TIA}}^2 K_c^2 + \frac{V_{n,\text{TIA}}^2}{(R_s + Z_{\text{in}})^2} + \frac{4k_B T}{R_s} \right) \quad (52)$$

which is also in unit W/Hz .

E. Noise factors

To enable a fair comparison between classical electronic receivers and quantum receivers, in this subsection, we compute the noise factors of quantum receivers by applying the Friis formulas for noise. Following the concept of quantum transconductance g_q , we treat the quantum receiver and the

photodiode as a quantum low-noise amplifier (qLNA) with noise factor

$$F_q = \frac{\text{SNR}_{\text{in}}}{\text{SNR}_{\text{out}}} = \frac{A_{\text{eq}} |E_{\text{sig}}|^2 / (2\eta_0 k_B T)}{(Lg_q |E_{\text{sig}}|)^2 / 4 / \text{PSD}[\Delta I_n]}, \quad (53)$$

where $A_{\text{eq}} = 3\lambda^2/(8\pi)$ is the equivalent aperture of a classical dipole antenna, and the output noise $\text{PSD}[\Delta I_n]$ contains the current PSD of BBR noise, photon shot noise, thermal noise of R_s , and the relative intensity noise of the probe laser set to be $\bar{I}_{\text{ph}}^2 \times (-140 \text{ dBc/Hz})$. The power gain of the qLNA is given by

$$G_q = \frac{(Lg_q |E_{\text{sig}}| K_c)^2 Z_{\text{in}} / 2}{|E_{\text{sig}}|^2 A_{\text{eq}} / (2\eta_0)}. \quad (54)$$

The noise factor and gain of the electronic TIA is given by

$$F_{\text{TIA}} = 1 + \frac{(I_{n,\text{TIA}} K_c)^2 / 2 + (V_{n,\text{TIA}} / (R_s + Z_{\text{in}}))^2 / 2}{\text{PSD}[\Delta I_n]}, \quad (55)$$

and the TIA power gain is

$$G_{\text{TIA}} = \frac{R_T^2}{Z_{\text{in}} R_L}. \quad (56)$$

By the Friis formulas for noise, the total power gain is $G = G_q G_{\text{TIA}}$, and the total noise factor is $F = F_q + (F_{\text{TIA}} - 1)/G_q$. The numerical results are shown in Fig. 5, where it can be seen that the minimum total noise factor of the quantum receiver is $F = 8.1 \text{ dB}$ achieved at $R_s = 4 \text{ k}\Omega$.

V. SIMULATION RESULTS

In this section, we present the simulation results of a Rydberg atomic receiver. The atomic receiver equips a cesium-133 atomic vapor cell of length $L = 2 \text{ cm}$, where the vapor cell is illuminated by a probe light at 852 nm with a probe power of $P_0 = 29.8 \mu\text{W}$ and a probe Rabi frequency of $\Omega_p = 2\pi \times 8.08 \text{ MHz}$. The counter-propagating control light at 510 nm is assumed to have a Rabi frequency of $\Omega_c = 2\pi \times 2.05 \text{ MHz}$ [37]. The value of the decay rates γ_i and the other parameters are aligned with [5]. The quantum

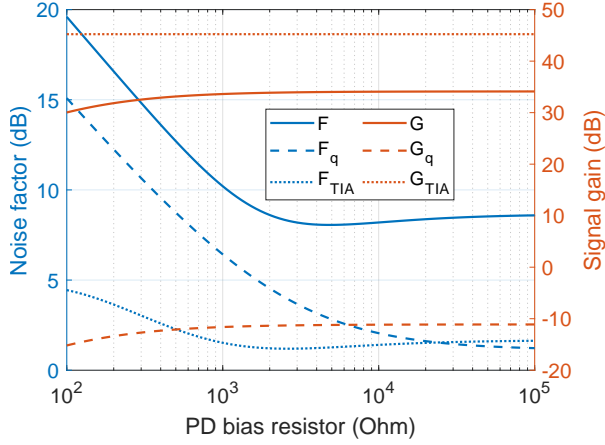


Fig. 5. Noise factor and power gain of the quantum LNA (qLNA) and the transimpedance amplifier (TIA) as a function of the PD bias resistor R_s .

TABLE I
COMMUNICATION SYSTEM PARAMETERS

Item	Value
Carrier frequency	6.9458 GHz
IF frequency f_{IF}	150 kHz
LO intensity E_{LO}	0.04 V/m
BS Tx power	20 dBm
BS Antenna gain	5 dB
Classical UE antenna gain	1.76 dB
BS-UE distance	1000 m
Symbol period	10 μ s
Runge-Kutta step size	1 ns

efficiency of the photodetector is set to be $\eta = 0.8$. All noises are evaluated at $T = 300$ K.

A. Dynamic results in the time domain

We first check the correctness of the small-signal transfer function (31) by simulating a single-carrier Rydberg atomic communication system. The simulated probe response of this atomic receiver is compared to that of the theoretically predicted response (31). The simulated probe response is obtained by applying an order-4 Runge-Kutta method to numerically solve the master equation (6). For the theoretical method, the transfer function is first calculated by evaluating (27) and (31), and then the transfer function is applied to the received E-field signal $E_{sig}(t)$ to theoretically compute the signal contained in $\text{Im}\{\rho_{21}\}(t)$. In both simulation and theoretical prediction, the probe response is computed by applying (4).

Figure 6 shows the simulated and theoretical dynamic response of the Rydberg atomic receiver to an information-carrying single-carrier communication signal. It can be seen that the dynamic component of the theoretical response well fits the simulated response.

B. Time-frequency results of the quantum transconductance

To better capture the input-output transition relationship of the Rydberg atomic receiver, in this subsection, we numer-

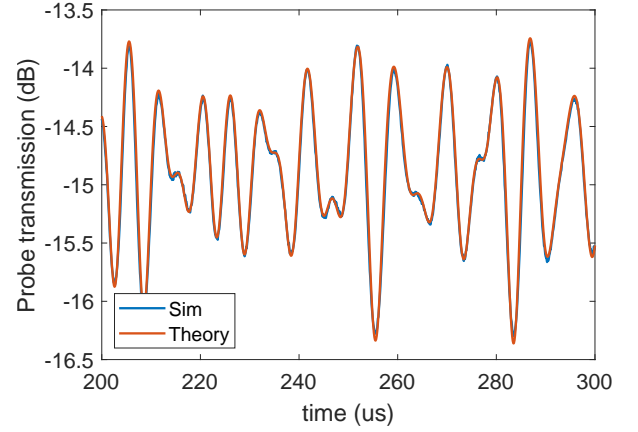


Fig. 6. Simulated and theoretically predicted probe responses to a single-carrier modulated signal.

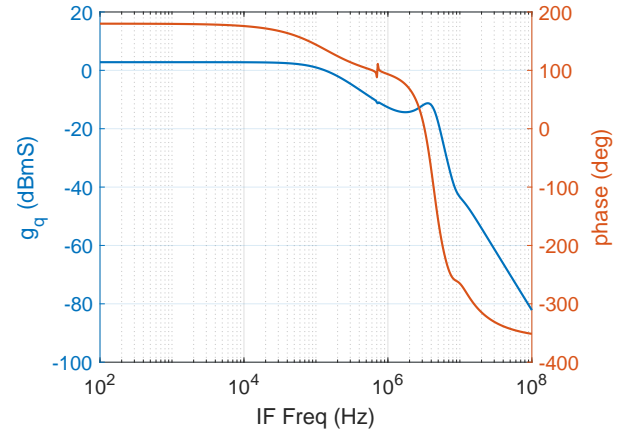


Fig. 7. Amplitude and phase responses of the quantum transconductance $g_q(i\omega)$.

ically compute the quantum transconductance in the time-frequency domain. Fig. 7 presents the amplitude and phase response of the quantum transconductance g_q as a function of the IF frequency f_{IF} .

Fig. 8 shows the impulse response and the step response of the quantum transconductance. A rise time of $t_r = 2.45 \mu\text{s}$ can be achieved, which corresponds to a 3 dB bandwidth of $\text{BW}_{3\text{dB}} = 0.35/t_r \approx 0.14 \text{ MHz}$, which is in agreement with the results of frequency-domain transconductance $g_q(i\omega)$. The theoretical single-sided instantaneous bandwidth value of about 0.1 MHz is also supported by experimental works [26, 45, 46]. Further bandwidth enhancement to 2.3 MHz is possible through cold atoms [29].

Fig. 9 shows the pole-zero map of the quantum transconductance $g_q(s)$. The quantum dynamic response is fully described by 15 poles, 13 zeros, and a DC gain $g_q(i0) = -1.4 \text{ mS}$ via the rational fraction factorization

$$g_q(s) = g_q(i0) \frac{\prod_{k=1}^{13} (1 - \frac{s}{z_k})}{\prod_{\ell=1}^{15} (1 - \frac{s}{p_\ell})}. \quad (57)$$

Note that all the poles and zeros are normalized by 2π to convert into frequency values.

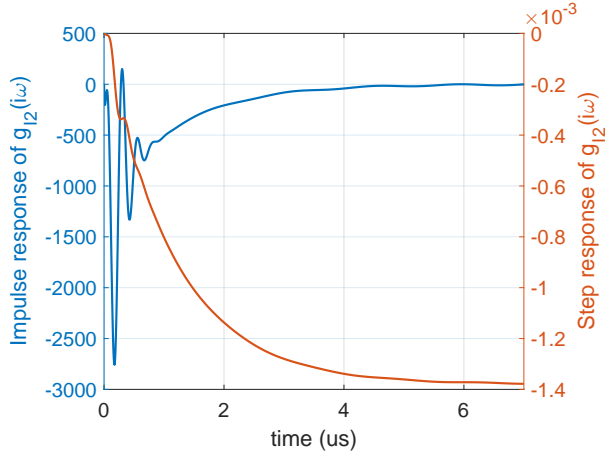


Fig. 8. Impulse response $g_q(x, \tau)$ and the corresponding step response $\int_0^t g_q(x, \tau) d\tau$ of the quantum transconductance as a function of time.

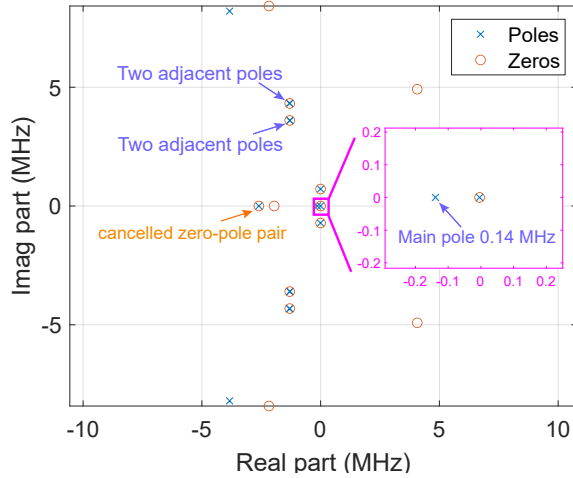


Fig. 9. Pole-zero map of the quantum transconductance $g_q(s)$.

C. Continuous-time simulation for wireless communications

To establish the complete wireless simulation link for the Rydberg atomic receiver, we perform downlink symbol transmission simulations by assuming a single-antenna BS serving a UE equipped with a single Rydberg atomic receiver. The channel model is assumed to be line-of-sight (LoS) with no obstacles and time-selective fading. At the Rydberg atomic receiver, the RF signal is first mixed by the LO signal with the Rydberg atoms, creating an optical IF signal with BBR noise PSD described by (46). After opto-electric conversion by the photodiode, this IF signal is amplified with a TIA, and then mixed with two orthogonal IF tones to down-convert the signal to the complex baseband.

The Tx/Rx waveforms and 16QAM constellations are shown in Fig. 10, with the imperfections in the received constellation attributed to the TIA electronic thermal noise, the BBR noise, the nonlinear effects of the Rydberg atom receiver, and the imperfect ISI suppression during single-carrier transmission. Detailed inspections of the contributions of these imperfections to the total error vector magnitude

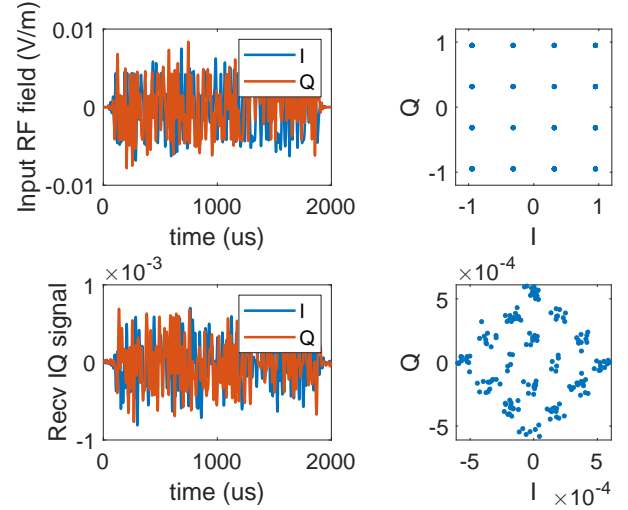


Fig. 10. Input noiseless RF waveform (analytic signal at f_{LO}) and the received noisy baseband complex signals, as well as their constellation representations. The estimated SNR is 17.71 dB from the Rx constellation.

(EVM) are beyond the scope of this theoretical paper, and are left for future works. From the results in Fig. 10, the Rx SNR is estimated to be 17.71 dB, and thus the equivalent noise PSD of the simulated Rydberg atomic receiver is estimated to be -152.0 dBm/Hz, which is about 22 dB above the thermal noise floor n_0 . This numerical result approximately coincides with the electric field measurement precision of $10.0 \text{ nV cm}^{-1} \text{ Hz}^{-1/2}$ reported in [29]. When we remove all the noise sources in the simulation, the estimated Rx SNR rises to 18.22 dB, which implies that the noise caused by systematic errors (symbol synchronization error, baseband pulse shaping error, atomic nonlinearity, etc.) in this simulation is larger than the BBR-induced noise plus the electronic thermal noise. If the quantum conductance g_q could be further improved by about 20 dB due to future experimental advancements, the photocurrent thermal noise is anticipated to be greatly suppressed. In this case, the BBR noise is expected to dominate the total system noise, where the system performance can finally achieve the bound (47).

D. Discrete-time baseband simulation for MIMO communications

In this subsection, we present the equivalent baseband model of the Rydberg superheterodyne receiver illustrated in Fig. 4. This baseband model can be directly extended to the MIMO case. By integrating all the dynamic signal models of each processing stage, the continuous-time equivalent baseband model is derived to be

$$y_{BB}(t) = \sqrt{\frac{P_T}{P_{qref}}} H x_{BB}(t) + w_{BB}(t), \quad (58)$$

where $x_{BB}(t)$ is the Tx complex baseband signal of unit power that lies within the 3 dB bandwidth of $g_q(i\omega)$, $y_{BB}(t)$ is the Rx complex baseband signal, H is the channel coefficient in the

usual sense², P_T [W] is the transmitted power of the classical transmitter, P_{qref} [W] is the quantum reference power level defined by

$$\frac{1}{\sqrt{P_{\text{qref}}}} = \frac{1}{2V_{\text{ref}}} R_T K_c L |g_q(i2\pi f_{\text{IF}})| \sqrt{\frac{8\pi\eta_0}{\lambda_c^2}}, \quad (59)$$

and $w_{\text{BB}}(t)$ is a complex white process within the instantaneous bandwidth upper-bounded by the bandwidth of $g_q(i\omega)$. The noise PSD is given by

$$\text{PSD}[w_{\text{BB}}(t)] = n_{\text{w,bb}} + n_{\text{w,shot}} + n_{\text{w,TIA}} + n_{\text{w,th}}, \quad (60)$$

where the components are computed to be

$$n_{\text{w,bb}} = \frac{1}{2} \left(\frac{1}{\sqrt{2}V_{\text{ref}}} (R_T K_c) L g_q \sqrt{\zeta(\ell)} \cdot \sqrt{2} E_{\text{n,bb}} \right)^2, \quad (61)$$

$$n_{\text{w,shot}} = \frac{1}{2} \left(\frac{1}{V_{\text{ref}}} (R_T K_c) \sqrt{2q_e \bar{I}_{\text{ph}}} \right)^2, \quad (62)$$

$$n_{\text{w,TIA}} = \frac{1}{2} \left(\frac{V_{\text{n,TIA}} R_T}{V_{\text{ref}} (Z_{\text{in}} + R_s)} \right)^2 + \frac{1}{2} \left(\frac{I_{\text{n,TIA}} K_c R_T}{V_{\text{ref}}} \right)^2, \quad (63)$$

$$n_{\text{w,th}} = \frac{1}{2} \left(\frac{K_c R_T}{V_{\text{ref}}} \sqrt{\frac{4k_B T}{R_s}} \right)^2. \quad (64)$$

The voltage V_{ref} is the reference voltage of the I/Q baseband ADC. We further assume a communication bandwidth W with the Tx baseband signal represented by $x_{\text{BB}}(t) = \sum_n x(n) \text{sinc}(Wt - n)$, then the continuous-time equivalent baseband model (58) is discretized into

$$y(n) = \sqrt{P_T/P_{\text{qref}}} H x(n) + w(n), \quad (65)$$

where $y(n) = y_{\text{BB}}(n/W)$, and $w(n)$ is an i.i.d. complex white Gaussian sequence of variance $\sigma_w^2 = W \cdot \text{PSD}[w_{\text{BB}}(t)]$ computed from (60). Note that the discrete-time signal model (65) can be easily extended to a MIMO signal model $\mathbf{y} = \sqrt{P_T/P_{\text{qref}}} \mathbf{H} \mathbf{x} + \mathbf{w}$ for each single MIMO channel use, or extended to a linear discrete-time multipath channel model $y(n) = \sqrt{P_T/P_{\text{qref}}} \sum_m H(m) x(n-m) + w(n)$, where $H(m)$ is the channel coefficient evaluated at the m -th tap.

Figure 11 shows the simulated 8×8 MIMO capacity for classical/quantum receivers with instantaneous bandwidth $B = 100$ kHz and Rayleigh channel fading. The noise factor of classical electronic receiver is set to be $F_c = 2$ dB. All the other simulation parameters are aligned to the previous continuous-time simulations. For the classical MIMO system, the Rx antenna mutual coupling (MC) effect is considered [47], resulting in a reduction of the received SNR and MIMO degrees-of-freedom (DoF). In contrast, the Rydberg atomic MIMO receiver is not susceptible to the antenna MC effect [15]. Thus, the quantum receiver outperforms the MC-influenced classical receiver. Moreover, it is expected that the quantum transconductance g_q could be further improved by approximately 20 dB [6, 30]. With this assumption, the

²The channel coefficient is canonically defined as the power-based transfer function s_{21} between the Tx isotropic antenna port and the Rx isotropic antenna port, evaluated at any specified frequency point within the communication bandwidth.

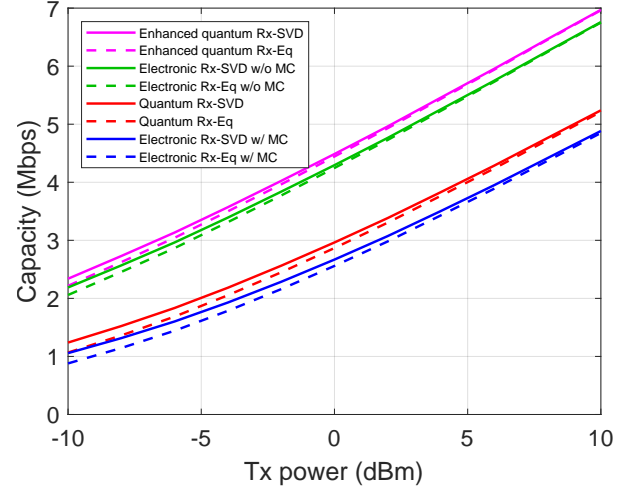


Fig. 11. MIMO capacity simulations for the quantum and classical receivers. “SVD” denotes water-filling power allocation across MIMO sub-channels with SVD-based Tx precoding/Rx combining, and “Eq” denotes equal power allocation.

enhanced quantum receiver could possibly outperform both the MC-free and the MC-influenced classical MIMO receivers. The enhancement of g_q , i.e., the enhancement of the intrinsic gain κ , can be realized by cooling the atomic gas [5, 29] or introducing RF resonant structures [48].

VI. CONCLUSIONS

In this paper, we provided a novel LTI system viewpoint for Rydberg atomic receivers by solving the Laplace domain transfer function directly from the physics-rooted master equation. With this LTI system viewpoint as well as the derived transfer functions, the atomic response to the signal field and the noise field can be readily computed in closed-form, which facilitates future study in Rydberg quantum communication and sensing systems. Finally, based on the signal and noise models, a single-carrier SISO/MIMO simulator for wireless communications was proposed, where the simulation results demonstrated the possibility of constructing a quantum MIMO receiver that outperforms classical electronic receivers.

Future works will be focused on experimental validation of the general signal model, and the integration of zero-IF architectures to further mitigate in-band BBR noise, bringing Rydberg atomic receivers closer to their theoretical performance limits.

VII. ACKNOWLEDGMENT

The authors would like to thank Prof. Wei E. I. Sha from Zhejiang University and Dr. Hanfeng Wang from Massachusetts Institute of Technology for their helpful discussions and constructive suggestions on Rydberg atomic receivers.

REFERENCES

- [1] M. A. Nielsen and I. L. Chuang, *Quantum computation and quantum information*. Cambridge university press, 2010.
- [2] N. Gisin and R. Thew, “Quantum communication,” *Nat. Photon.*, vol. 1, no. 3, pp. 165–171, Mar. 2007.
- [3] V. Scarani, H. Bechmann-Pasquinucci, N. J. Cerf, M. Dušek, N. Lütkenhaus, and M. Peev, “The security of practical quantum key

- distribution,” *Rev. Mod. Physics*, vol. 81, no. 3, pp. 1301–1350, Mar. 2009.
- [4] C. L. Degen, F. Reinhard, and P. Cappellaro, “Quantum sensing,” *Rev. Mod. Physics*, vol. 89, no. 3, p. 035002, Mar. 2017.
 - [5] M. Jing, Y. Hu, J. Ma, H. Zhang, L. Zhang, L. Xiao, and S. Jia, “Atomic superheterodyne receiver based on microwave-dressed Rydberg spectroscopy,” *Nat. Physics*, vol. 16, no. 9, pp. 911–915, Sep. 2020.
 - [6] T. Gong, J. Sun, C. Yuen, G. Hu, Y. Zhao, Y. L. Guan, C. M. S. See, M. Debbah, and L. Hanzo, “Rydberg atomic quantum receivers for classical wireless communications and sensing: Their models and performance,” arXiv preprint arXiv:2412.05554, Dec. 2024.
 - [7] M. Cui, Q. Zeng, and K. Huang, “Towards atomic MIMO receivers,” *IEEE J. Sel. Areas Commun.*, vol. 43, no. 3, pp. 659–673, Mar. 2025.
 - [8] Y. Chen, X. Guo, C. Yuen, Y. Zhao, Y. L. Guan, C. M. S. See, M. Debbah, and L. Hanzo, “Harnessing Rydberg atomic receivers: From quantum physics to wireless communications,” arXiv preprint arXiv:2501.11842, Jan. 2025.
 - [9] H. Gray and C. Stroud Jr., “Autler-Townes effect in double optical resonance,” *Optics Commun.*, vol. 25, no. 3, pp. 359–362, Mar. 1978.
 - [10] C. L. Holloway, J. A. Gordon, A. Schwarzkopf, D. A. Anderson, S. A. Miller, N. Thairachoen, and G. Raithel, “Sub-wavelength imaging and field mapping via electromagnetically induced transparency and Autler-Townes splitting in Rydberg atoms,” *Appl. Physics Lett.*, vol. 104, no. 24, Jun. 2014.
 - [11] H. Fan, S. Kumar, J. Sedlacek, H. Kübler, S. Karimkashi, and J. P. Shaffer, “Atom based RF electric field sensing,” *J. Physics B*, vol. 48, no. 20, p. 202001, Sep. 2015.
 - [12] K. Yang, X. Chen, R. Mao, J. Li, and Y. Fu, “PCB-based electrically tunable resonator for VHF band Rydberg atomic enhancement sensing,” *IEEE Trans. Antennas Propagat.*, vol. 72, no. 7, pp. 6060–6068, Jul. 2024.
 - [13] S. Berweger, N. Prajapati, A. B. Artusio-Glimpse, A. P. Rotunno, R. Brown, C. L. Holloway, M. T. Simons, E. Imhof, S. R. Jefferts, B. N. Kayim *et al.*, “Rydberg-state engineering: Investigations of tuning schemes for continuous frequency sensing,” *Phys. Rev. Appl.*, vol. 19, no. 4, p. 044049, Apr. 2023.
 - [14] Y.-Y. Lin, Z.-Y. She, Z.-W. Chen, X.-Z. Li, C.-X. Zhang, K.-Y. Liao, X.-D. Zhang, J.-H. Chen, W. Huang, H. Yan *et al.*, “Terahertz receiver based on room-temperature Rydberg-atoms,” *Fundamental Research*, Mar. 2023.
 - [15] S. S. Yuan, X. Y. Xu, J. Yuan, G. Xie, C. Huang, X. Chen, Z. Huang, and W. E. Sha, “Electromagnetic modeling and capacity analysis of Rydberg atom-based MIMO system,” *IEEE Ant. Wirel. Propagat. Lett.*, Mar. 2025.
 - [16] H. Zhang, Y. Ma, K. Liao, W. Yang, Z. Liu, D. Ding, H. Yan, W. Li, and L. Zhang, “Rydberg atom electric field sensing for metrology, communication and hybrid quantum systems,” *Sci. Bulletin*, vol. 69, no. 10, pp. 1515–1535, Oct. 2024.
 - [17] F. Zhang, B. Jin, Z. Lan, Z. Chang, D. Zhang, Y. Jiao, M. Shi, and J. Xiong, “Quantum wireless sensing: Principle, design and implementation,” in *Proc. 29th Annual Int. Conf. Mobile Comput. Netw. Association for Computing Machinery*, Jan. 2023.
 - [18] E. Graham, S. Ghosh, Y. Zhu, X. Bai, S. B. Cahn, E. Durcan, M. J. Jewell, D. H. Speller, S. M. Zacarias, L. T. Zhou *et al.*, “Rydberg-atom-based single-photon detection for haloscope axion searches,” *Phys. Rev. D*, vol. 109, no. 3, p. 032009, Mar. 2024.
 - [19] M. Cui, Q. Zeng, Z. Wang, and K. Huang, “Realizing quantum wireless sensing without extra reference sources: Architecture, algorithm, and sensitivity maximization,” arXiv preprint arXiv:2504.21234, Apr. 2025.
 - [20] S. H. Autler and C. H. Townes, “Stark effect in rapidly varying fields,” *Physical Review*, vol. 100, no. 2, p. 703, Feb. 1955.
 - [21] J. A. Gordon, C. L. Holloway, S. Jefferts, and T. Heavner, “Quantum-based SI traceable electric-field probe,” in *2010 IEEE Int. Symp. Electro. Compat.* IEEE, Jan. 2010, pp. 321–324.
 - [22] J. A. Sedlacek, A. Schwettmann, H. Kübler, R. Löw, T. Pfau, and J. P. Shaffer, “Microwave electrometry with Rydberg atoms in a vapour cell using bright atomic resonances,” *Nat. Phys.*, vol. 8, no. 11, pp. 819–824, Aug. 2012.
 - [23] M. Schmidt, S. Bohaichuk, V. Venu, F. Christaller, C. Liu, F. Ripka, H. Kübler, and J. P. Shaffer, “Rydberg-atom-based radio-frequency sensors: Amplitude-regime sensing,” *Opt. Express*, vol. 32, no. 16, pp. 27 768–27 791, Jul. 2024.
 - [24] Y. Cai, S. Shi, Y. Zhou, Y. Li, J. Yu, W. Li, and L. Li, “High-sensitivity Rydberg-atom-based phase-modulation receiver for frequency-division-multiplexing communication,” *Phys. Rev. Appl.*, vol. 19, no. 4, p. 044079, Apr. 2023.
 - [25] J. Yuan, T. Jin, L. Xiao, S. Jia, and L. Wang, “A Rydberg atom-based receiver with amplitude modulation technique for the fifth-generation millimeter-wave wireless communication,” *IEEE Ant. Wirel. Propagat. Lett.*, vol. 22, no. 10, pp. 2580–2584, Oct. 2023.
 - [26] D. A. Anderson, R. E. Sapiro, and G. Raithel, “An atomic receiver for AM and FM radio communication,” *IEEE Trans. Antenna Propagat.*, vol. 69, no. 5, pp. 2455–2462, May 2020.
 - [27] C. L. Holloway, M. T. Simons, A. H. Haddab, J. A. Gordon, D. A. Anderson, G. Raithel, and S. Voran, “A multiple-band Rydberg atom-based receiver: AM/FM stereo reception,” *IEEE Antennas Propagat. Mag.*, vol. 63, no. 3, pp. 63–76, Mar. 2020.
 - [28] C. L. Holloway, M. T. Simons, J. A. Gordon, and D. Novotny, “Detecting and receiving phase-modulated signals with a Rydberg atom-based receiver,” *IEEE Ant. Wirel. Propagat. Lett.*, vol. 18, no. 9, pp. 1853–1857, Sep. 2019.
 - [29] H.-T. Tu, K.-Y. Liao, H.-L. Wang, Y.-F. Zhu, S.-Y. Qiu, H. Jiang, W. Huang, W. Bian, H. Yan, and S.-L. Zhu, “Approaching the standard quantum limit of a Rydberg-atom microwave electrometer,” *Sci. Adv.*, vol. 10, no. 51, p. eads0683, Dec. 2024.
 - [30] F.-C. Wu, Q. An, J.-W. Yao, and Y.-Q. Fu, “Research on intrinsic expansion coefficients in Rydberg atomic heterodyne receiving link,” *Acta Physica Sinica*, vol. 72, no. 4, Apr. 2023.
 - [31] M. Cui, Q. Zeng, and K. Huang, “Multi-user SIMO wireless communications based on atomic receivers,” in *Proc. IEEE Global Commun. Conf.* IEEE, Dec. 2024, pp. 4101–4106.
 - [32] F. Wu, Q. An, Z. Sun, and Y. Fu, “Linear dynamic range of a Rydberg-atom microwave superheterodyne receiver,” *Phys. Rev. A*, vol. 107, no. 4, p. 043108, Apr. 2023.
 - [33] M. Cui, Q. Zeng, and K. Huang, “MIMO precoding for Rydberg atomic receivers,” arXiv preprint arXiv:2408.14366, Aug. 2024.
 - [34] M. Schmidt, S. Bohaichuk, V. Venu, F. Christaller, C. Liu, F. Ripka, H. Kübler, and J. P. Shaffer, “Rydberg-atom-based radio-frequency sensors: Amplitude-regime sensing,” *Opt. Express*, vol. 32, no. 16, pp. 27 768–27 791, Jul. 2024.
 - [35] M. T. Simons, A. H. Haddab, J. A. Gordon, and C. L. Holloway, “A Rydberg atom-based mixer: Measuring the phase of a radio frequency wave,” *Appl. Phys. Lett.*, vol. 114, no. 3, Mar. 2019.
 - [36] R. Sapiro, G. Raithel, and D. Anderson, “Time dependence of Rydberg EIT in pulsed optical and RF fields,” *J. Physics B*, vol. 53, no. 9, p. 094003, Sep. 2020.
 - [37] L. Zhang, Y. Jia, M. Jing, L. Guo, H. Zhang, L. Xiao, and S. Jia, “Detuning radio-frequency electrometry using Rydberg atoms in a room-temperature vapor cell,” *Laser Phys.*, vol. 29, no. 3, p. 035701, Mar. 2019.
 - [38] S. M. Bohaichuk, D. Booth, K. Nickerson, H. Tai, and J. P. Shaffer, “Origins of Rydberg-atom electrometer transient response and its impact on radio-frequency pulse sensing,” *Phys. Rev. Appl.*, vol. 18, no. 3, p. 034030, Sep. 2022.
 - [39] D. Bertilone, “Spatial behavior of the coherence tensors for blackbody radiation emission,” *J. Optical Soc. America*, vol. 14, no. 2, pp. 497–509, Feb. 1997.
 - [40] R. Carminati and J.-J. Greffet, “Near-field effects in spatial coherence of thermal sources,” *Phys. Rev. Lett.*, vol. 82, no. 8, p. 1660, Feb. 1999.
 - [41] J. Zhu, Z. Wan, L. Dai, and T. J. Cui, “Electromagnetic information theory-based statistical channel model for improved channel estimation,” *IEEE Trans. Inf. Theory*, vol. 71, no. 3, pp. 1777–1793, Mar. 2025.
 - [42] Z. Wan, J. Zhu, Z. Zhang, L. Dai, and C.-B. Chae, “Mutual information for electromagnetic information theory based on random fields,” *IEEE Trans. Commun.*, vol. 71, no. 4, pp. 1982–1996, Apr. 2023.
 - [43] C. T. Fancher, D. R. Scherer, M. C. S. John, and B. L. S. Marlow, “Rydberg atom electric field sensors for communications and sensing,” *IEEE Trans. Quantum Eng.*, vol. 2, pp. 1–13, Mar. 2021.
 - [44] *Variable Gain High Speed Current Amplifier*, FEMTO, Nov. 2010. [Online]. Available: https://www.aps.anl.gov/files/APS-Uploads/DET/Detector-Pool/Electronics/Amplifiers/dhpc-100_r9_Datasheet.pdf
 - [45] A. Deb and N. Kjærgaard, “Radio-over-fiber using an optical antenna based on Rydberg states of atoms,” *Appl. Phys. Lett.*, vol. 112, no. 21, May 2018.
 - [46] H. Li, J. Hu, J. Bai, M. Shi, Y. Jiao, J. Zhao, and S. Jia, “Rydberg atom-based AM receiver with a weak continuous frequency carrier,” *Opt. Express*, vol. 30, no. 8, pp. 13 522–13 529, Apr. 2022.
 - [47] J. W. Wallace and M. A. Jensen, “The capacity of MIMO wireless systems with mutual coupling,” in *Proc. IEEE 56th Veh. Tech. Conf.*, vol. 2. IEEE, Sep. 2002, pp. 696–700.
 - [48] G. Sandidge, G. Santamaria-Botello, E. Bottomley, H. Fan, and Z. Popović, “Resonant structures for sensitivity enhancement of Rydberg-atom microwave receivers,” *IEEE Trans. Microwave Theory and Tech.*, vol. 72, no. 4, pp. 2057–2066, Apr. 2024.